


Molecular thermodynamics of complex coacervate systems. Part II: Measuring and modeling of the phase envelope using pePC-SAFT

Moreno Ascani^a, Wojciech P. Lipiński^b, Iris B.A. Smokers^b, Piramsuya Neethirajah^a, Max Vogel^a, Evan Spruijt^b, Gabriele Sadowski^a, Christoph Held^{a,*} 

^a Laboratory of Thermodynamics, Department of Biochemical and Chemical Engineering, TU Dortmund University, Emil-Figge Str. 70, 44277 Dortmund, Germany

^b Radboud University, Institute for Molecules and Materials, Heyendaalseweg 135, 6525 Nijmegen, the Netherlands

ARTICLE INFO

Keywords:

Polyelectrolytes
NADH
Protamine
Poly-L-lysine
LLPS

ABSTRACT

Complex coacervation is an associative liquid-liquid phase separation (LLPS) observed in aqueous solutions of oppositely charged polyions. Coacervates are relevant systems in biology, chemistry, food and cosmetics industry, medicine as well as in engineering e.g. as extracting agents, for drug delivery or as gelling, foaming or stabilizing agents. Unfortunately, accurate experimental data on equilibrium compositions of complex coacervates are still scarce in the literature. Here, the LLPS of the coacervate-forming system water-Na₂NADH-protamine sulfate was measured at $T = 298.15$ K and $p = 1.013$ bar and at different polycation/polyanion ratios. Qualitative features of the experimental phase envelope are carefully discussed based on molecular interactions in this system. Compared to equilibrium data of the system water-Na₂NADH-poly-L-lysine HBr, the system water-Na₂NADH-protamine sulfate revealed a larger miscibility gap, suggesting a strong contribution of non-coulombic interactions to the phase behavior of this coacervate system. Experimental data were successfully modeled using the recently developed pePC-SAFT (Ascani et al., Part 1, *Fluid Phase Equilibria*, under review). The pePC-SAFT predicted phase envelope was in very good agreement with the measured experimental points. To the best of our knowledge, this is the first time that a physically sound model was used to model the phase envelope of a biologically relevant complex coacervate system.

1. Introduction

Complex coacervation is an associative liquid-liquid phase separation (LLPS) observed in aqueous solutions of oppositely charged polyions [1,2]. Representative of such class of systems are aqueous solutions of proteins-polysaccharides [3,4], of proteins-nucleotides [5–7] or of synthetic polyelectrolytes [8–11]. The complex coacervate phase is highly enriched in both polyions which are present in a concentration ratio close to the stoichiometric charge ratio (i.e. the concentration ratio of polyanion and polycation at which their respective charges are balanced) and with an overall mass fraction between 0.15 - 0.35 g per gram (see, for example, the measurements of Spruijt *et al.* [10], of Bohidar *et al.* [12] and of Mathieu *et al.* [13]), while the diluted phase (supernatant phase) contains the solutes (both polyions and their counterions) at a much lower concentration than the coacervate phase. The phenomenological origin of complex coacervation was reviewed in our previous work (Ascani *et al.*, Part 1, *Fluid Phase Equilibria*, under

review) and was extensively discussed in recent reviews [1,2,14].

An emerging research area for which complex coacervation plays an important role is the study and synthesis of artificial cells, as well as the understanding and mimic of structures and processes in real cells. This interest in coacervates was promoted by the discovery of several membraneless organelles (MLOs) in the interior of living cells. MLOs are droplets of a liquid phase, enriched in macromolecules, dispersed within the cell cytoplasm and nucleoplasm. The biggest MLO is the nucleolus, discovered as early as 1830, which is present inside the cell nucleus and is enriched in RNA and proteins [15]. In 2009, Brangwynne discovered that Germline P granules exhibits liquid-like behavior, like fusion and wetting, and that they rapidly dissolve and condense [16]. Stress granules, which are cellular organelles that subtract RNA from the cytoplasm and which are formed under stress conditions, resemble the structure of P granules and are MLOs formed by RNA and proteins, as discovered in 2013 [17]. Other examples of MLOs include Cajal, cleavage and PML bodies in the nucleus, as well as germ granules and RNA transport

* Corresponding author.

E-mail address: christoph.held@tu-dortmund.de (C. Held).

<https://doi.org/10.1016/j.fluid.2024.114305>

Received 20 September 2024; Received in revised form 10 November 2024; Accepted 30 November 2024

Available online 5 December 2024

0378-3812/© 2024 The Authors. Published by Elsevier B.V. This is an open access article under the CC BY license (<http://creativecommons.org/licenses/by/4.0/>).

granules in the cytoplasm [18].

Those discoveries prove that LLPS (most of which in biology are complex coacervates) is a more ubiquitous phenomenon in life science than previously supposed. MLOs allow a highly increased concentration of components within the cell while maintaining molecular mobility. This enables boosting reactions in these sub-compartments which would not be favored in too diluted conditions [15]. The function of some MLOs may also be to sequester molecules and thus inhibiting their reactivity in the cell interior, as has been attributed to stress and RNA transport granules [18,19]. Another advantage of MLOs is the fast dynamics of their formation and regulation, which can be tuned by minute switching of physical parameters such as pH, concentration, ionic strength, pressure or temperature [18]. This mechanism of cellular compartmentalization by LLPS may have served as a primordial form of molecular assembly in the emergence of early life on earth [16]. Oparin [20] first proposed that a premise for the origin of life, in the diluted primordial broth, was a local enrichment and organization of small molecules into protocells. He further proposed complex coacervation as a means of achieving the high local concentration of macromolecules that promoted self-replicating structures. Meanwhile, it is known that complex coacervates are capable of enriching complex, charged molecules which are essential for the development of life, such as lysozymes [21] or RNA [22]. LLPS formed by complex coacervates are further recognized as an ideal platform for artificial cells, as they mimic the crowded, viscous and charged nature of the cytoplasm [23].

Technical applications of complex coacervates include their potential use as extracting agents, for example to sequester and concentrate biomolecules from a fermentation broth [24–26], as materials to design microcapsules and nanoparticles for drug delivery [27–30] or as gelling, foaming or stabilizing agents in the food and cosmetic industry [31–33]. The requirement of accurate experimental phase equilibrium data and predictive models is therefore a mandatory task, as mentioned by Sing et al. [1,2].

The first experimental work on a complex coacervate system is credited to Bungenberg de Jong [34–36], who compiled the first documented extensive investigation of complex coacervation by studying the LLPS in the aqueous system gum arabic-gelatin. Bohidar et al. [12] investigated the composition of the coacervate phase in the aqueous system bovine serum albumin-poly(diallyldimethylammonium) (PDADMA) chloride using UV-Vis spectroscopy and size-exclusion chromatography. Spruijt et al., [10] firstly performed quantitative investigation of the phase behavior of complex coacervates in an aqueous system of synthetic polyelectrolytes. The authors measured the salt concentration versus molarity diagrams of poly(acrylic acid) (PAA) and poly(N,N-dimethylaminoethyl methacrylate) (PDMAEMA), in 1:1 stoichiometric ratio, by labeling PAA with fluorescein and measuring its concentration, in both phases, by UV-Vis spectroscopy. The same concentration of PDMAEMA and PAA in both phases, as well as equal partitioning of the small counterions between the coacervate phase and the supernatant phase was assumed in their work. The phase envelope was modeled with the Voorn-Overbeek model. In two subsequent works, Chollakup et al. [8,9] investigated the phase behavior of the complex coacervate formed by the synthetic polyelectrolytes sodium polyacrylate and poly(allyl amine) hydrochloride in water. They investigated different mixing ratios of the polyanion and the polycation in the phase envelope and different molecular weights, as well as phase envelopes at different values of salt concentration, temperature and pH. The different salt-polyanion-polycation composition points were classified as either “solution” (homogeneous), “coacervate” or “precipitate” by turbidity and optical microscopy analysis. Li et al. [37] performed a similar experiment as Spuijt et al. by quantitatively measuring the phase equilibrium over salt concentration of the two oppositely charged polypeptides poly-L-lysine and poly-D,L-glutamic acid of same chain length, using thermogravimetric analysis. They could also measure the salt concentration in both phases and concluded that salts tend to preferentially partition into the supernatant phase. Recently, Neitzel et al. [38]

performed extensive quantitative phase equilibrium measurements on systems containing two differently functionalized and oppositely charged poly(allyl glycidyl ethers) using thermogravimetric analysis. By varying the degree of functionalization of both coacervate-former components, they could elucidate for the first time the effect of the charge density on the resulting LLPS of complex coacervates. Wang et al. [39] investigated the phase envelope of the system composed of PDMAEMA and a negatively charged coordination polymer formed from zinc and a bis-ligand L₂EO₄ [1,11-bis(2,6-dicarboxypyridin-4-yloxy)–3,6,9-trioxaundecane]. The concentration of PDMAEMA and L₂EO₄ in both phases was measured by ¹H-NMR and the phase envelope was quantitatively constructed by measuring the coexisting concentrations of the polyions at different mixing ratios. Moreover, the effect of zinc on the coacervate formation and its partitioning in both phases were also investigated. Koga et al. [40] investigated complex coacervate systems formed by poly-L-lysine with different numbers of L-lysine monomers \bar{n} as polycation and several nucleotides (ATP, ADP, AMP, GTP, CTP, TTP, UTP) as the polyanionic counterpart. Their investigation of the phase equilibrium was of qualitative character: the influence of nucleotide concentration, pH and temperature on coacervate formation was investigated by monitoring the change in absorption intensity at fixed wavelength. Cakmak et al. [22] measured turbidities of complex coacervates in the aqueous system poly-L-lysine and poly-L-arginine (with number of arginine monomers \bar{n} between 1 and 100) with the nucleotides ATP, ADP and AMP, as well as poly-L-aspartic and poly-L-glutamic acids (chain length between 1 and 100 as well). Smokers et al. [6] investigated the coacervate system of poly-L-lysine and poly-L-arginine (both with $\bar{n} = 10$) in water with several metabolites having two or more negative charges, by measuring the critical salt concentration at fixed metabolite and polycation concentration. Wang et al. [41] measured the molar polycation-polyanion ratio in the coacervate phase of the system polystyrene sulfate (PSS) - PDADMA using 600 MHz ¹H-NMR spectroscopy.

Among all these experimental results on the phase equilibrium of complex coacervates, only the work of Spruijt et al. [10], Chollakup et al. [8,9], Wang et al. [39], Li et al. [37], and Neitzel et al. [38] have attempted a systematic mapping of the phase envelopes. Moreover, phase equilibrium data of biologically relevant systems are completely missing in the literature. This might be due to the higher availability of synthetic polyelectrolytes, the poorly defined physicochemical properties of naturally derived macromolecules, and the very strong non-coulombic interactions (particularly hydrogen bonds, π - π -interactions, dispersion interactions) among biologic macromolecules, which are difficult to separate from the purely coulombic interactions that prevail in classical synthetic polyelectrolytes (and thus make the comparison with theories, such as the Voorn-Overbeek model, more complicated).

The goal of this work is to fill the research gap on measuring and modeling LLPS of biologically relevant complex coacervates. In this work we aimed at a) measuring quantitatively the phase equilibrium of the system water-Na₂NADH-protamine sulfate and b) modeling this system using pePC-SAFT, an Equation of State (EoS) which was revised and developed in our previous work (Ascani et al., Part 1, *Fluid Phase Equilibria*, under review) to model complex coacervates.

2. Materials and methods

Chemicals: Chemicals used in this work were Na₂NADH (β -nicotinamide adenine dinucleotide reduced disodium salt hydrate), protamine sulfate, poly-L-lysine HBr, tris(hydroxymethyl)aminomethane (TRIS), Trizma hydrochloride (TRIS-HCl), Bradford reagent. All the chemicals were used without purification.

Na₂NADH (CAS No 606–68–8) was purchased from Carl Roth. Na₂NADH dissociates into Na⁺ and NADH²⁻ upon dissolution in water, with NADH²⁻ having a pK_a = 4.01 at T = 298.15 K and p = 1.013 bar (thus carrying two negative charges at a neutral pH). Poly-L-Lysine HBr

(CAS No 25,988–63–0) with a molecular weight between 30,000–70,000 Da (corresponding to 140–330 lysine monomers) was purchased from Sigma Aldrich. Protamine sulfate from salmon (CAS No 53,597–25–4) was purchased from Sigma Aldrich. Through our work, Trizma buffer with a concentration of 10 mM and a pH of 7.6, prepared from the Tris base and Tris–HCl, was used to prepare and dilute the samples and stock solutions of Na₂NADH, protamine sulfate and poly-L-lysine HBr.

Stock solutions of 100 mmol·kg⁻¹ Na₂NADH and stock solutions of 6 mmol·kg⁻¹ protamine sulfate were prepared each in 10 mM Trizma buffer with a pH value adjusted to 7.6. The stock solution of Na₂NADH was kept frozen upon utilization, while the stock solution of protamine sulfate was stored at 4 °C. The stock solution of protamine sulfate was heated at 40 °C and sonicated for 10 min before utilization to ensure homogeneity of the solution. The preparation of the stock solutions and samples containing poly-L-lysine as well as the experimental methodology to evaluate compositions in the system water–Na₂NADH–poly-L-lysine are explained in the Supporting Information (S.I.). The methodology to record confocal microscopy images of heterogeneous samples of the system water–Na₂NADH–protamine sulfate is explained in the S.I. as well.

Location of the miscibility gap in the system water–Na₂NADH–protamine sulfate: To obtain an initial estimation of the location of the miscibility gap in the system water–Na₂NADH–protamine sulfate, the composition space was screened and turbidity of samples at different compositions was assessed by evaluating the extinction of each sample at 600 nm. 36 composition points were chosen in a 6 × 6 matrix in a concentration range between 0.035 and 0.8 mmol·kg⁻¹ of protamine sulfate and between 1 and 20 mmol·kg⁻¹ of Na₂NADH. For the measurement of each point, aliquots of 240 μL were prepared at each composition. For the measurements of the absorbance, a TECAN plate reader was used (Tecan Spark M10). Results of the turbidity analysis are shown in Fig. S-1.

Preparation and analysis of the samples in the system water–Na₂NADH–protamine sulfate: For the sample preparation, first the weight of one falcon tube of 15 mL volume was recorded. Then aliquots of stock solutions of Na₂NADH, protamine sulfate and of Trizma buffer 10 mM were added in the falcon tube, according to the target concentration of NADH²⁻ and protamine, up to a total sample volume of 10 mL. After shaking for 20 s, the sample was left in a water bath at 25 °C for 20 min. The sample was then centrifuged, at 25 °C and 4000 rpm, for 30 min. After centrifugation, the supernatant was withdrawn by pipette and stored in a 2 mL Eppendorf tube before analysis. The falcon tube with the remaining coacervate phase was then re-centrifuged for 5 min under the same conditions (4000 rpm and 25 °C) to remove all the traces of supernatant from the wall of the tube. Afterwards, the remaining of the supernatant and part of the coacervate phase close to the interface were removed and the weight of the falcon tube with the remaining coacervate phase was recorded. The weight of the remaining coacervate phase was calculated as the difference between the weight of the falcon tube with the coacervate and the initial weight of the empty falcon tube. The coacervate phase was then redissolved by adding 6000 mg of a 50 mM NaCl solution (the exact amount of the added NaCl solution was weighted and recorded) and then stored for further analysis. In general, the amount of coacervate phase which was collected was between 40 and 120 mg (from an initial, total sample volume of 10 mL) for all the feed compositions investigated in this work.

The samples of supernatant and dissolved coacervate phase were analyzed by means of quantitative NMR spectroscopy. For the determination of the concentration of both the NADH²⁻ and protamine in the samples, ³¹P and ¹H-NMR spectra were recorded in a Bruker-AVANCE III 500 spectrometer at 500 MHz, using phosphonoacetic acid and 3-(trimethylsilyl) propionic-2,2,3,3-*d*₄ acid sodium salt (TMS-*d*₄) as the respective reference internal standard. The aqueous samples were mixed with D₂O in a 9:1 ratio, and a solvent suppression sequence was used in the recording of the spectra. One representative spectrum of a protamine solution obtained in this work, which is in excellent agreement to the

500 MHz ¹H-NMR spectrum of protamine in D₂O reported by Gucinski et al. [42], is shown in Fig. S-2.

The concentration of NADH²⁻ was calculated from the signal intensity of the phosphor atoms (2 atoms) of the two phosphate groups, while the concentration of protamine was calculated from the signal intensity of the two hydrogens in δ-position of the arginine (42 atoms). Calculation of the concentrations (in molality, mmol·kg⁻¹) was performed, from the signal intensity *I* of the component *c* and of the internal standard *I*_{IS} and the known concentration of internal standard \tilde{m}_{IS} , using Eq. (1) [43].

$$\frac{\tilde{m}_c N^c}{\tilde{m}_{IS} N^{IS}} = \frac{I_c}{I_{IS}} \quad (1)$$

In Eq. (1), *N* represents the number of atoms (of the target component or internal standard) responsible for the signal. All the spectra were evaluated in MestReNova 14. The procedure of sample preparation and measurement of both phases was independently replicated 3 times for each feed point investigated in this work, and the standard deviation of the final concentration was determined. Values of the concentration of NADH²⁻ and protamine in both phases and for different feed compositions are reported in Table S-2.

As validation of the sample preparation and of the analytical method employed in this work, we measured the water content in the coacervate phase (which is the most difficult to measure) by a gravimetric method. For this we prepared, in triplicate, 5 mL buffer samples containing 0.8 mmol·kg⁻¹ Na₂NADH and 10 mmol·kg⁻¹ protamine sulfate in glass tubes. The glass tubes were previously dried in an oven at 120 °C for four days and regularly weighted to ensure a stable weight of each tube. The sample preparation procedure, including centrifugation and the separation of the supernatant phase, was the same as the procedure for sample preparation in the falcon tubes for the NMR analysis. The glass tubes with the coacervate phase were then weighted again and left in an oven at 120 °C for twelve days while regularly being weighted to ensure a stable weight at the end of the drying. The water content was calculated as the difference between the weight of each sample before and after drying, divided by the total weight of the coacervate phase after preparation of the samples. The water content was calculated from the NMR-measured concentrations of NADH²⁻ and protamine in the coacervate phase and their molecular weight. It was assumed in this procedure that the mass of the remaining coacervate phase mainly consisted of water (masses of counterions and other species were neglected).

Within the standard deviation of the triplicate measurements of each method, they show remarkable agreement (The gravimetrically determined concentration of dry mass is 0.514±0.016 g·g⁻¹ whereas the concentration determined by NMR is 0.522±0.017 g·g⁻¹), thus confirming the reliability of the adopted sample preparation and NMR analysis.

Measurement of osmotic coefficients of water–protamine sulfate solutions: Osmotic coefficients (OC) of solutions of water–protamine sulfate were measured at a concentration of protamine sulfate up to 3 mmol·kg⁻¹ and performed in triplicate. A freezing point osmometer (Osmomat 010, Gonotec GmbH, Berlin, Germany) was used after previous calibration with aqueous NaCl solutions from Gonotec. Osmotic coefficients were calculated from the measured osmolality *osmol* of the solution using Eq. (2).

$$OC = \frac{osmol}{(\nu_{SO_4^{2-}} + \nu_{Prot}) \tilde{m}_{Prot}} \quad (2)$$

Where $\nu_{SO_4^{2-}}$ and ν_{Prot} denote, respectively, the number of moles of sulfate anions (10.5) and protamine polycations (1) present in one mole of protamine sulfate. The values of the osmotic coefficients of the investigated samples and the concentration of protamine sulfate are reported in Table S-1.

3. pePC-SAFT: modeling approach and model parameters

In this work, pePC-SAFT as proposed in our previous work (Ascani et al., Part 1, *Fluid Phase Equilibria*, under review) was used to model osmotic coefficients of polyelectrolyte solutions and LLPS of water-Na₂NADH-protamine sulfate. pePC-SAFT is an equation of state based on perturbation theory [44], according which a separation of contributions in the intermolecular interaction potential translates (at least conceptually) exactly into a separation of contributions to the residual Helmholtz energy a^{res} according to Eq. (3).

$$a^{res} = \frac{A^{res}}{Nk_B T} = a^{hs} + a^{ion} + a^{ch,hc} + a^{disp} + a^{assoc} + a^{Born} \quad (3)$$

In Eq. (3), $a^{ch,hc}$ represent the charged hard-chain energy contribution, which is a perturbation of the charged hard-sphere fluid described by the first two terms ($a^{hs} + a^{ion}$). Assumption and simplifications in this term were extensively described in our previous work (Ascani et al., Part 1, *Fluid Phase Equilibria*, under review). Counterion condensation and electrostatic association between oppositely charged polyions is treated as an association between charged spheres within the Wertheim TPT1 theory, thus by the association term a^{assoc} , as explained in our previous work as well.

In this and our previous work (Ascani et al., Part 1, *Fluid Phase Equilibria*, under review) the influence of the Born term and of the relative dielectric constant on the LLE of complex coacervate systems was tested and no qualitative difference was found between both strategies (with and without Born term). The reason for this is the great water content in both phases, which results in a marginal decrement of the dielectric constant from the supernatant to the coacervate phase, regardless of the mixing rule (and the exact value of the relative dielectric constant of polyions and counterions) employed in the estimation of the relative dielectric constant. The value of the dielectric constant of the counterions was set to that of water, which reduces our modeling strategy to our previous approach described in Held et al. [45]. In alignment to our previous approach, the dispersion energy between like-charged small counterions (for instance, between two Na⁺ ions) was set to zero. However, the dispersion energy between like-charged polyions and polyions-counterions (for instance, protamine-protamine or protamine-Na⁺) was considered. This is due to the fact that in the highly concentrated coacervate phase coulombic forces (both attractive AND repulsive) are highly screened and therefore short-range non-coulombic forces become dominant even between like-charged polyions.

The amino-acid sequence of protamine from salmon was investigated by Gucinski et al. [42], who reported that one molecule of protamine from salmon contains 32 amino acids, among which 21 arginine, 4 serine, 3 proline, 2 glycine, 1 leucine and 1 alanine groups. This sequence was used for the parametrization of protamine (explained in the remaining of this section) and for all the calculations within this work. Among the 32 amino acids in the protamine, only the arginine can be protonated due to the free guanidinium group which carries a positive charge under physiological pH. The amide bonds between amino acids are not protonated, and the free end amino group of proline and carboxyl group of arginine in the protamine were not considered, since both are oppositely charged in the investigated pH condition and therefore do not contribute to the overall charge of protamine. The amount of sulfate in the protamine was assumed to be 10.5 ions pro protamine molecules (and this value was used for phase equilibrium calculations in this work), as required to neutralize the overall charge of the protamine. NADH²⁻ carries two negative charges at physiological pH. In this work, NADH²⁻ and protamine were described as heterosegmental chains. Thus, NADH²⁻ and protamine have two domains each with its own set of pure-component and binary interaction parameters. Only one of the domains carries the charges of the respective molecule. NADH²⁻ was parametrized in a previous work by Greinert et al. [46] using ePC-SAFT, but neither PC-SAFT nor ePC-SAFT parameters of

protamine were available in the literature. The parameters of the small ions (Na⁺ and SO₄²⁻), either pure-component parameters (shown in Table 1) or binary interaction parameters (shown in Table 2) were inherited from Held et al. [45]. In this work, parameters of NADH²⁻ and protamine were fitted, using pePC-SAFT, to osmotic coefficients and, for protamine, also to LLE of binary mixtures water-protamine sulfate, under the constraint given by Eq. (4).

$$m_{i,1}\sigma_{i,1}^3 + m_{i,2}\sigma_{i,2}^3 = const \quad (4)$$

Eq. (4) can be interpreted as the excluded volume of species i and was found to correlate well with the liquid density of pure specie i or its mixtures (see, for example, the work of Tihic et al., [47]), meaning that different values of m and σ giving the same $const$ value in Eq. (4) will likely predict very similar values of the liquid density at the same conditions. The $const$ value in Eq. (4) was determined, for NADH²⁻, from the homosegmental parametrization of Greinert et al. [46] (thus, for NADH²⁻, $const = m \cdot \sigma^3$, with m and σ as the segment number and segment diameter of NADH²⁻ from the work of Greinert). For protamine, this value was determined as the sum of the contribution of the 32 amino acids which were parametrized by Held et al. [48] using PC-SAFT (thus, for protamine, $const = \sum_i m_i \sigma_i^3$, where the sum goes over all the 32 amino acid present in protamine, and m_i and σ_i being, respectively, the segment number and segment diameter of each of the amino acids in protamine, taken from the work of Held et al. [48]). The dispersion-energy parameter u_{NADH} of NADH²⁻, as well as the association scheme and parameters, was inherited from the old parametrization of Greinert et al. [46]. The dispersion-energy parameter u_{Prot} of protamine was estimated from the dispersion-energy parameter of the single amino acids in the parametrization of Held, according to the correlation given by Eq. (5).

$$m_{Prot,1}\sigma_{Prot,1}^2 u_{Prot} + m_{Prot,2}\sigma_{Prot,2}^2 u_{Prot} = \sum_i m_i \sigma_i^2 u_i \quad (i = \text{amino acid}) \quad (5)$$

In Eq. (5), the sum on the right-hand side runs over all the 32 amino acids forming the protamine. Furthermore, for protamine, an association scheme was employed to mimic the strong π - π interactions among guanidinium groups, between guanidinium groups and NADH²⁻, as well as to describe the competitive interaction of water with the guanidinium groups. Those competitive interactions were investigated by molecular simulation [49], which found stacking and aggregation of adjacent protamine molecules [50] up to LLPS in aqueous solutions of protamine sulfate [51]. In this work, 110 donor sites were assigned to the domain 1 of protamine (allowing five water molecules to associate to each of the 21 guanidinium groups, 1 water molecule to each of the four serine and one water molecule to the terminal proline of the protamine molecule). Since it is supposed, from molecular simulation, that two guanidiniums can undergo ion pairing by expelling two water molecules [49], 42 acceptor sites (i.e. two acceptors for each of the 21 guanidinium in the protamine) were further assigned to the domain 2 of protamine and are only allowed to associate with the 110 donor sites on domain 1 (but not with association sites on water). The 110 donor sites can associate with water as well as with the 42 acceptor sites, thus characterizing the competitive hydration-dehydration and π - π interactions of guanidinium groups. To describe π - π interactions in presence of NADH²⁻, four further donor sites were assigned to the latter, which were allowed to associate only to one of the 42 acceptors of the protamine on domain 2. The association-energy parameter ϵ^{Aibi}/k_B of the 42 acceptor sites on the protamine as well as the binary interaction parameter k_{ij} between protamine and water (the same value of the binary interaction parameter k_{ij} between water and both domains of protamine was used) were adjusted to the experimental LLE data of protamine sulfate and water (see Fig. 2b)); the resulting ϵ^{Aibi}/k_B from this fitting was then used as the association energy of the four donor sites on NADH²⁻ that can associate with the 42 acceptors of protamine. The ϵ^{Aibi}/k_B of the 110 donor sites of protamine was set to 2500 K., because it was mainly the difference

Table 1

Pure-component parameters used in this work. The values in brackets (see protamine, domain 1, NADH²⁻, domain 1, and SO₄²⁻) are parameters of the “charged” association sites which describe counterion condensation.

Component	m_i^{seg}	$\sigma_i / \text{\AA}$	$u_i / k_B / K$	N / -	$\epsilon^{AIBi} / k_B / K$	$\kappa^{AIBi} / -$	$z_i / -$	$\epsilon_{r,i} / -$	Ref.
Protamine (domain 1)	60.903	4.120	522.278	110:0 (7)	2500.0 (8000)	0.038 (0.004)	21	30*	This work
Protamine (domain 2)	9.997	4.120	522.278	0:42	1280.0	0.038	0	30*	This work
NADH ²⁻ (domain 1)	1.000	2.756	380.520	4:0 (2)	1280.0 (0.0)	0.001 (0.004)	-2	30*	This work
NADH ²⁻ (domain 2)	16.139	3.247	380.520	8:8	3711.9	0.001	0	30*	This work
Water	1.2047	*1	353.950	1:1	2425.7	0.04509	0	78.5	[52]
Na ⁺	1	2.823	230.000	-	-	-	1	-*	[45]
SO ₄ ²⁻	1	2.649	80.000	(2)	-	(0.004)	-2	-*	[45]

*The ϵ_r of Na⁺ and SO₄²⁻ was set to that of water, which reduces our modeling strategy to our previous approach described in Held *et al.* [45]; the ϵ_r of Protamine and NADH²⁻ was set to 30, which is in the range of the ϵ_r of common functionalized organic components. The final ϵ_r is estimated from the $\epsilon_{r,i}$ of each component by a segment-based mixing rule.

Table 2

Binary interaction parameters used in this work. In brackets: binary interaction parameters which correct for the cross-association energy according to the Berthelot-Lorenz combining rules (these binary interaction parameters, however, do not apply for association between charged hard-spheres).

$k_{ij,298.15 K} / -(\kappa^{AIBi} / -)$	Protamine (domain 1)	Protamine (domain 2)	NADH ²⁻ (domain 1)	NADH ²⁻ (domain 2)	Water	Na ⁺	SO ₄ ²⁻
Protamine (domain 1)	-	0.00	-0.0063 (1.00)	-0.0063 (1.00)	0.07	0.00	0.00
Protamine (domain 2)	-	-	-0.0063 (-0.045)	-0.0063 (1.00)	0.07 (1.00)	0.00	0.00
NADH ²⁻ (domain 1)	-	-	-	0.00	0.00 (1.00)	0.00	0.00
NADH ²⁻ (domain 2)	-	-	-	-	0.00	0.00	0.00
Water	-	-	-	-	-	0.00045 [45]	0.25 [45]
Na ⁺	-	-	-	-	-	-	-1.00 [45]
SO ₄ ²⁻	-	-	-	-	-	-	-

between the association strength of association and donor sites that influenced the calculation results.

Counterion condensation between the positively charged protamine and the negatively charged SO₄²⁻ was described, according to our previous work (Ascani *et al.*, Part 1, *Fluid Phase Equilibria*, under review), by allowing cross-association interactions between both oppositely charged ions, where the number of “charged” association sites on protamine was adjusted to the experimental osmotic coefficients (Fig. 2a) of aqueous solutions of protamine sulfate. The number of those association sites on SO₄²⁻ that can associate with protamine was set to two. To mimic the competitive counterion condensation in presence of the negatively charged NADH²⁻, the latter are given two “charged” association sites as well, which can only associate with the “charged” sites on domain 1 of protamine (thus in competition with SO₄²⁻).

Binary interaction parameters between protamine and NADH²⁻ were fitted to one tie-line of the ternary system water-Na₂NADH-protamine

sulfate. Pure component and binary interaction parameters used in this work are reported, respectively, in Tables 1 and 2.

Fig. 1 reports the experimental and predicted osmotic coefficients and density of the system water-Na₂NADH and Fig. 2 reports experimental and predicted osmotic coefficients and LLE of the system water-protamine sulfate. Osmotic coefficients were calculated from the activity coefficient of water γ_w (calculated with pePC-SAFT) at the given conditions and the water concentration x_w using Eq. (6).

$$OC = \frac{\ln \gamma_w x_w}{\ln x_w} \quad (6)$$

It must be mentioned that the new parameters of NADH²⁻ were only fitted to osmotic coefficients (diagram of Fig. 1a) whereas the density (diagram of Fig. 1b)) is only predicted as a validation of the employed correlation given by Eq. (4). We expect a similar result for protamine, whose parameters contain the volumetric information of the

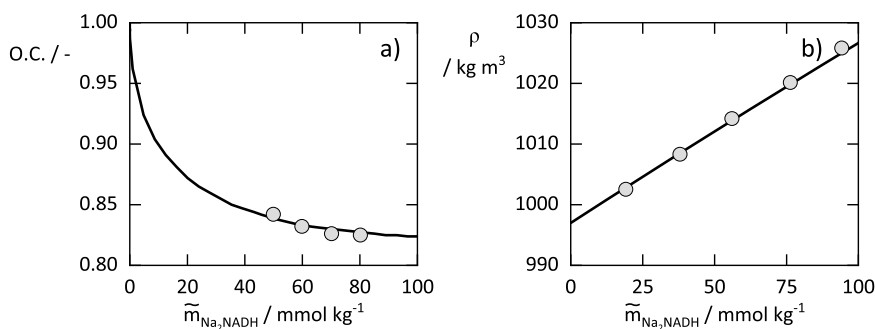


Fig. 1. Osmotic coefficients at $T = 303.15$ K and $p = 1.013$ bar (diagram a) and densities at $T = 298.15$ K and $p = 1.013$ bar (diagram b)) of aqueous solutions of Na₂NADH at different concentrations. Solid lines are calculated with pePC-SAFT with NADH²⁻ parameters from Tables 1 and 2, symbols are experimental results from Wangler *et al.* [53].

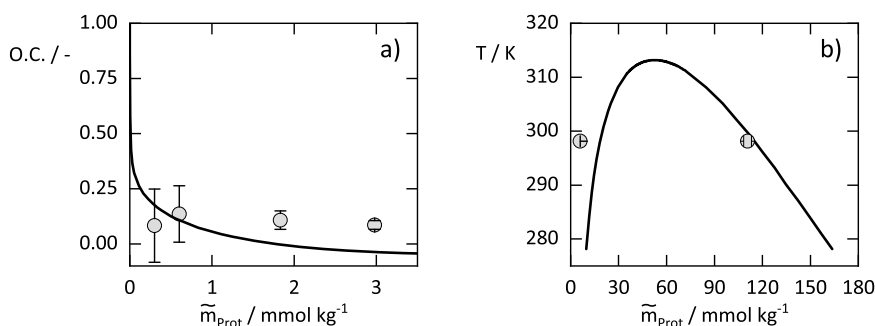


Fig. 2. Osmotic coefficients at $T = 298.15$ K and 1 bar (diagram a)) and binary LLE at 1 bar (diagram b)) of aqueous solutions of protamine sulfate. Solid lines are calculated with pePC-SAFT using parameters from Tables 1 and 2, symbols are experimental results determined in this work, which are reported in Table S1.

constituting amino acids via the same correlation.

4. Results and discussion

Validation of experiments: complex coacervation in the system water- Na_2NADH -protamine sulfate occurred, after mixing both stock solutions of Na_2NADH and protamine sulfate, as a white emulsion finely dispersed in the whole volume of the system. After thermal equilibration and centrifugation, the settled coacervate phase appeared as a limpid, yellow droplet of a highly viscous liquid. The lighter supernatant, settled above the coacervate phase, appeared transparent and colorless, except at the very high Na_2NADH concentration where it took a slightly yellow color. The dispersed two-phase system after mixing, as well as the settled system after centrifugation, are shown in Fig. 3.

The relatively weak charge density of NADH^{2-} and protamine, compared to other systems from the literature [10], likely prevents irreversible precipitation and thus formation of solid complexes. Fig. 4 shows pictures of confocal microscope of two coacervate samples, containing $10 \text{ mmol} \cdot \text{kg}^{-1}$ of Na_2NADH and, respectively, $0.4 \text{ mmol} \cdot \text{kg}^{-1}$ and $0.8 \text{ mmol} \cdot \text{kg}^{-1}$ of protamine sulfate. The confocal microscopy images reveal the homogeneous and liquid-like nature of the coacervate droplet, thus corroborating our presumption that the system does not undergo irreversible precipitation, and that the system rapidly reaches thermodynamic phase equilibrium after phase separation.

Experimental and predicted projected phase envelope: the concentrations of NADH^{2-} and of protamine on points of the coexisting supernatant and coacervate phases at equilibrium are reported in diagrams a) and b) of Fig. 5. In diagram a), experimental equilibrium-composition

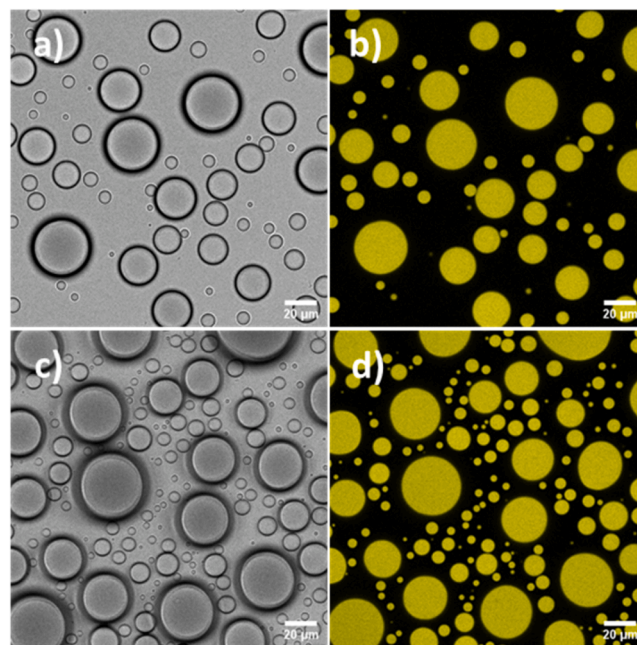


Fig. 4. Confocal microscopy images of two samples containing 10 mM of Na_2NADH and, respectively, 0.4 mM (images a) and b)) and 0.8 mM (images c) and d)) of protamine sulfate. Images b) and d) show the corresponding fluorescence from the protamine labelled with NHS-rhodamine. The methodology for sample preparation and confocal microscopy is given in the S.I.

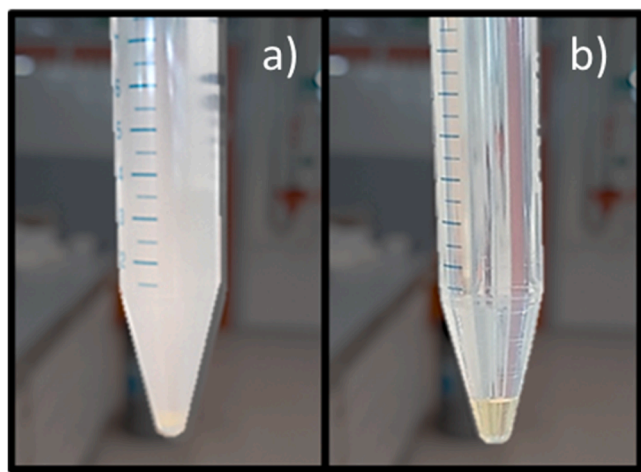


Fig. 3. Images of a coacervate sample after mixing aliquots of stock solutions of both Na_2NADH and protamine sulfate (picture a) and after centrifugation of the sample (picture b)), with both the coacervate phase (small volume of a yellow liquid in the bottom) and the supernatant phase clearly visible.

points in the coacervate (supernatant) phase are reported as yellow (gray) points. Both phases are connected by a solid black line. For the concentration representation as those in Fig. 5, the term “tie-line” must not be used since the concentration of only three of the five components can be read from the diagrams while information (concentration) of the counterions is missing in this representation. Prediction of pePC-SAFT according to the modeling strategy presented in the previous sections are reported, in diagram a), as points connected by lines as well as points along a pseudo-binodal curve (where, again, the concentration of the counterions cannot be read). Diagram b) of Fig. 5 also shows the used feed compositions, which are represented as green stars for each experimental feed point, and as green lines for the manifold of feed points used to perform the LLE flash calculations (from which the pseudo-binodal result). The importance of providing the overall feed composition for such systems was extensively discussed in our previous work (Ascani et al., Part 1, *Fluid Phase Equilibria*, under review) and is due to the fact that, in a 5-component electrolyte system, 3 independent variables need to be provided, at given temperature and pressure, to uniquely specify the system. Only a 3D diagram which represents, for instance, the concentration of polyanion, polycation and both

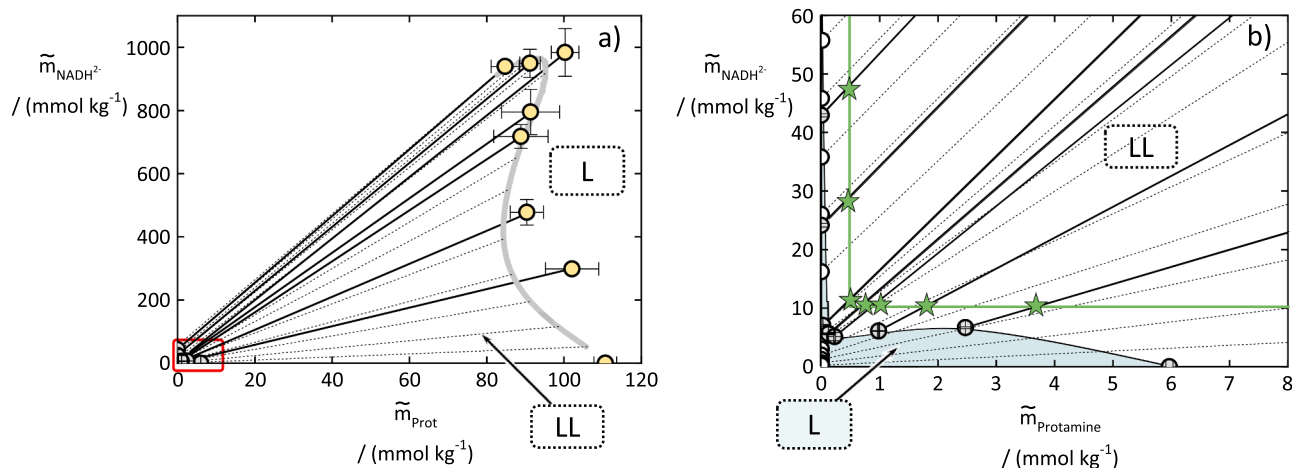


Fig. 5. Projected phase envelope of the coacervate system water- Na_2NADH -protamine sulfate at 298.15 K and 1.013 bar. Diagram a) shows the experimentally determined coexisting concentrations at equilibrium of both NADH^{2-} and protamine (in $m\tilde{m} = \text{mmol}\cdot\text{kg}^{-1}$), in the coacervate phase (yellow points) as well as in the supernatant (gray points), which are connected by a black, solid line; the dashed lines and the thick gray line represent, respectively, calculated coexisting compositions at equilibrium and the pseudo-binodal curve predicted by pePC-SAFT. Diagram b) shows an enlargement of the diluted supernatant phase (corresponding to an enlargement of the red square in the diagram a)) with the used experimental feed compositions (green stars), the one-phase region (blue area marked by the text field 'L') as well as the two-phase region (white area marked by the text field 'LL'); represented are some compositions predicted by pePC-SAFT (white points connected by dashed lines); the two green vertical and horizontal lines represent the manifold of all feed points used to perform the LLE flash calculation (and therefore to calculate the coexisting compositions reported in both diagrams as well as the pseudo-binodal curve). The solid curve connecting the experimental concentration points (gray points) in the supernatant is only intended to guide the eyes reader.

counterions can thus provide the full specification of the system (such as diagram a) of Fig. 7 from Ascani et al., Part 1, *Fluid Phase Equilibria*, under review). A 2D representation such as diagrams a) and b) of Fig. 5 is not complete, since any information about the counterions is missing: different concentration of the counterions lead in general to a different extent of phase separation and thus to different concentration of the polyions in both phases. Providing the overall feed composition removes this ambiguity (the exact concentration of the counterions in each phase, however, is still missing in this representation).

As can be seen from Fig. 5a and b, the system water- Na_2NADH -protamine sulfate shows an overlapping of two different topologies of phase diagrams: one "classical" LLPS of a pseudo-binary system (water-protamine sulfate) and the isolated miscibility gap of a complex coacervate system. LLPS in an aqueous solution of a single polyelectrolyte is a rather rare phenomenon, due to the high entropic penalty upon phase separating the small ions into the second phase. This entropic penalty is reduced when the counterion is divalent, as it is in protamine sulfate, due to the lower molar fraction (at the same charge concentration) and the stronger tendency of multivalent counterions to bond to the polyionic chain (see the equation of the Flory-Huggins mixing entropy, i.e. Eq. (5) from Ascani et al., Part 1, *Fluid Phase Equilibria*, under review). An important role in the LLPS of protamine sulfate in water, which is already reported in the literature [51], is played by the strong tendency of the positively charged guanidinium groups in protamine sidechains to form symmetric ion pairs (i.e. with both pairing ions having the same charge) by expelling two water molecules [49,51], as discussed in the previous section.

In the "complex coacervate region" (the central region of the projected phase envelope of Fig. 5a), the values of the concentration of protamine and NADH^{2-} in the coacervate phase tend to remain similar in magnitude, i.e. different overall mixing ratios of both polyions in the system barely affects their concentration in the coacervate phase (at least considering the concentration of charges from NADH^{2-} and protamine, as will be discussed later in this section). However, this is not valid for the supernatant where almost any concentration ratio of both polyions is observed, as can be seen from Fig. 5b. A similar finding was reported by Wang et al. [39], who found a close-to-stoichiometric concentration ratio of both polyions in the coacervate phase but (dependent on the overall mixing ratio) a much more varying concentration ratio in

the supernatant. In our work, the NADH^{2-} concentration in the supernatant tends to remain above $\sim 5 \text{ mmol}\cdot\text{kg}^{-1}$ at any feed composition (except, of course, at the pseudo-binary system water-protamine sulfate) whereas the protamine is almost completely depleted from the supernatant at high NADH^{2-} concentration. As discussed in our previous publication (Ascani et al., Part 1, *Fluid Phase Equilibria*, under review), this asymmetry in the concentration can be explained by the Flory-Huggins mixing entropy and the different sizes of NADH^{2-} and protamine, according to which the entropic penalty of removing a certain volume fraction of a large molecule (which in the investigated system is protamine) is lower than removing the same volume fraction of smaller molecules. The almost complete depletion of protamine from the supernatant is correctly reproduced by pePC-SAFT, as can be seen in Fig. 5b; however, the increase of protamine concentration in the supernatant, which was detected experimentally when the concentration of NADH^{2-} in the supernatant reaches $\sim 5 \text{ mmol}\cdot\text{kg}^{-1}$, could not be predicted by pePC-SAFT using the employed modeling strategy and the parameter set in Tables 1 and 2.

The greatest concentration of both polyions in the coacervate phase (and therefore the greatest size of the miscibility gap) is observed at the feed ratio $\tilde{m}_{\text{protamine}}/\tilde{m}_{\text{NADH}} = 0.4 \text{ mmol}\cdot\text{kg}^{-1}/10 \text{ mmol}\cdot\text{kg}^{-1}$, and decreases at other feed compositions. Fig. 6 reports the same phase envelope as Fig. 5a but represented in terms of charge-based molality (i.e. number of moles of positive or negative charges per kg of water) of protamine and NADH^{2-} . A closer inspection into the projected phase envelope of Fig. 6 reveals that at the maximal extent of phase separation (and highest concentration of both NADH^{2-} and protamine in the coacervate phase) both components are present, in the coacervate phase, in stoichiometric ratio, meaning that the positive charges of protamine are balanced by the negative charges of NADH^{2-} . Therefore, bringing an excess of one of the counterions in the coacervate phase (which has a high entropic penalty compared to separating the polyions, as explained in our previous work) is not required to maintain electroneutrality. However, this situation changes upon varying the protamine/ NADH^{2-} ratio, since if this ratio is different from the stoichiometric, more counterions are required in the coacervate phase to maintain electroneutrality, which at the end will reduce the size of the miscibility gap. This behavior is also reproduced by pePC-SAFT: the size of the miscibility gap is predicted to be at its maximum when both, NADH^{2-} and

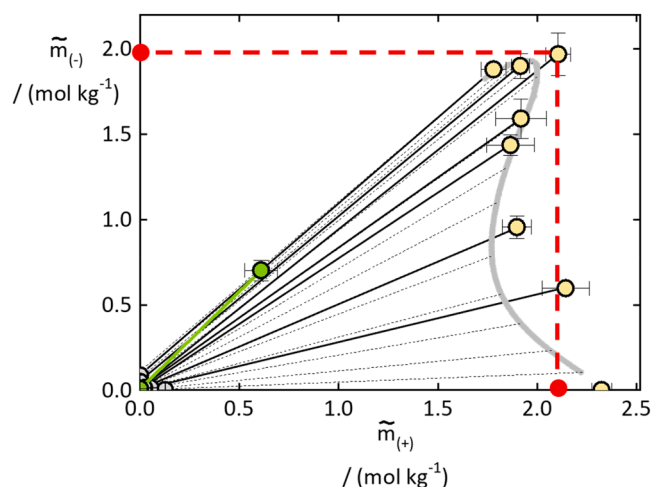


Fig. 6. Projected phase envelope of the system water- Na_2NADH -protamine sulfate at 298.15 K and 1.013 bar, where the number of moles of charges per kg of water of either NADH^{2-} (-) or protamine (+) is used as concentration unit. Dashed, red lines are projections of the charge concentrations to the respective axes and serve to highlight the near-to stoichiometric charge ratio from NADH and protamine in the coacervate phase (except at high protamine concentration). In the bottom-left of the diagram, the green line which connects two green circles represents the coexisting compositions of the coacervate and supernatant of one feed point of the system water- Na_2NADH -poly-L-lysine HBr.

protamine, are present in stoichiometric ratio in the coacervate phase. The quantitative composition of the coacervate phase predicted by pePC-SAFT is in very good agreement with experiments, as can be seen from Figs. 5a and 6, showing small deviations for feed composition at high protamine concentration.

Fig. 6 shows, furthermore, two composition points corresponding to the coacervate and supernatant phases of the system water- Na_2NADH -poly-L-lysine HBr at equilibrium, displayed as green circles connected by a green line. Compared to the size of the miscibility gap in the system water- Na_2NADH -protamine sulfate, the system water- Na_2NADH -poly-L-lysine HBr shows a lower extent of phase separation, which reflects the absence of π - π -interactions between lysine and NADH^{2-} .

Partitioning of small ions: Fig. 7 shows the concentration of poly-L-lysine, NADH^{2-} and Br^- in the supernatant and in the whole system that corresponds to the single feed point reported in Fig. 6. The great separation of poly-L-lysine from the supernatant into the coacervate phase can be observed, which agrees with the observation in the system

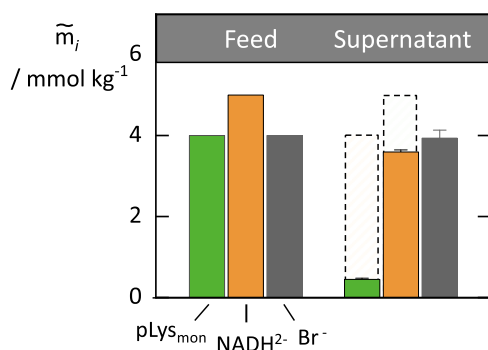


Fig. 7. Diagram showing, in the system water- Na_2NADH -poly-L-lysine HBr at 298.15 K and 1.013 bar, the overall molality of NADH^{2-} , poly-L-lysine (in term of monomer concentration) and bromide anion in the investigated feed point and the molality of the same species in the supernatant. Bars with dashed border serve only to compare the concentrations in the supernatant with overall concentrations in the system. The experimental methodology used to perform those measurements as well as the measured concentration values are reported in the S.I.

water- Na_2NADH -protamine sulfate where protamine, i.e. the largest macromolecule in the system, is almost completely depleted from the aqueous solution in the complex coacervate region. On the other hand, we found that the small Br^- anion remains almost completely in the supernatant and does not tend to preferential partition in one specific phase. We suppose a similar partitioning behavior, in the complex coacervate region of the system water- Na_2NADH -protamine, for both counterions Na^+ and SO_4^{2-} . Our calculation predicts indeed a slighter higher partitioning of SO_4^{2-} in the coacervate phase, where both NADH^{2-} and protamine remain the prevalent component in a close-to-stoichiometric ratio. At the high protamine concentration close to the binary system water-protamine sulfate, however, the NADH^{2-} in the coacervate phase tends to be substituted by the SO_4^{2-} , according to our calculation. This is reflected by the flatter slope of the lines connecting the composition of both phases in Figs. 5 and 6.

5. Conclusion

In this work, the equilibrium concentration of NADH^{2-} and protamine in the ternary complex coacervate system water- Na_2NADH -protamine sulfate was measured at different feed compositions, ranging from the pure binary system water-protamine sulfate up to high concentrations of Na_2NADH . A robust method was employed for the preparation, separation, and analysis of the composition of both the equilibrated supernatant phase and coacervate phase, which was cross-validated by a gravimetric method. Differently from most of the systems studied in the literature, this complex coacervate system shows an overlapping of two different topologies of LLPS: complex coacervation when the concentration of NADH^{2-} and protamine is comparable, and a “classical” LLPS of a (pseudo)binary system (water-protamine sulfate) at a high protamine/ NADH^{2-} ratio. In the “complex coacervation” region, NADH^{2-} and protamine show a concentration ratio close to stoichiometric in the coacervate phase, whereas in the supernatant protamine tends to be almost completely depleted at a high NADH^{2-} concentration. One single feed point of the system water- Na_2NADH -poly-L-lysine HBr was measured. Compared to the system water- Na_2NADH -protamine sulfate, the former shows a much lower phase separation, confirming the strong, non-coulombic contribution of π - π -interaction between protamine and NADH^{2-} to the phase behavior of the latter system.

The EoS pePC-SAFT, developed in our previous work to describe complex coacervate systems, was used in this work to model the system water- Na_2NADH -protamine sulfate. Both protamine and NADH^{2-} were modeled as heterosegmental hard chains containing one charged and one neutral domain. Counterion condensation was modeled as association between the charged segments of protamine and the SO_4^{2-} according to our previous work. An association scheme that reflects the competitive association of guanidium groups of arginine, water and NADH^{2-} was employed. Pure-component and binary interaction parameters of NADH^{2-} and protamine were fitted to osmotic coefficients and, for protamine, to the binary LLE in the system water-protamine sulfate as well. Only two binary interaction parameters between protamine and NADH^{2-} were fitted to one experimental tie-line of the system water- Na_2NADH -protamine sulfate. The resulting prediction of pePC-SAFT was very accurate in almost the entire composition range of protamine and NADH^{2-} and for both the supernatant and coacervate phase. An exception was the supernatant at low NADH^{2-} concentration, where the experimentally observed concentration of protamine was underestimated by pePC-SAFT. Nevertheless, this work showcases the potential of a physical sound model to model and predict the phase behavior of complex coacervate systems where coulombic and non-coulombic interactions may strongly affect the LLPS and partitioning of the constituting components.

CRedit authorship contribution statement

Moreno Ascari: Writing – original draft, Visualization, Software,

Methodology, Investigation, Formal analysis, Data curation, Conceptualization. **Wojciech P. Lipiński**: Methodology, Investigation. **Iris B.A. Smokers**: Supervision, Methodology, Investigation, Conceptualization. **Piramsuya Neethirajah**: Investigation. **Max Vogel**: Investigation. **Evan Spruijt**: Writing – review & editing, Supervision, Project administration. **Gabriele Sadowski**: Writing – review & editing, Supervision, Funding acquisition. **Christoph Held**: Writing – review & editing, Supervision, Project administration, Methodology, Formal analysis, Conceptualization.

Declaration of competing interest

The authors declare that they have no known competing financial interests or personal relationships that could have appeared to influence the work reported in this paper.

Acknowledgement

The authors acknowledge funding from the Deutsche Forschungsgemeinschaft (DFG, German Research Foundation) under Germany's Excellence Strategy-EXC 2033-project number 390677874. Translation into German required: "Gefördert durch die Deutsche Forschungsgemeinschaft (DFG) im Rahmen der Exzellenzstrategie des Bundes und der Länder-EXC 2033-Projektnummer 390677874-RESOLV".

Supplementary materials

Supplementary material associated with this article can be found, in the online version, at [doi:10.1016/j.fluid.2024.114305](https://doi.org/10.1016/j.fluid.2024.114305).

Data availability

The experimental data is in the SI.

References

- [1] C.E. Sing, Development of the modern theory of polymeric complex coacervation, *Adv. Colloid. Interface. Sci.* 239 (2017) 2–16.
- [2] C.E. Sing, S.L. Perry, Recent progress in the science of complex coacervation, *Soft. Matter.* 16 (12) (2020) 2885–2914.
- [3] C.G.de Kruijf, F. Weinbreck, R.de Vries, Complex coacervation of proteins and anionic polysaccharides, *Curr. Opin. Colloid. Interface. Sci.* 9 (5) (2004) 340–349.
- [4] S.L. Turgeon, C. Schmitt, C. Sanchez, Protein–polysaccharide complexes and coacervates, *Curr. Opin. Colloid. Interface. Sci.* 12 (4–5) (2007) 166–178.
- [5] K.K. Nakashima, J.F. Baaij, E. Spruijt, Reversible generation of coacervate droplets in an enzymatic network, *Soft. Matter.* 14 (3) (2018) 361–367.
- [6] I.B.A. Smokers, M.H.I. van Haren, T. Lu, E. Spruijt, Complex coacervation and compartmentalized conversion of prebiotically relevant metabolites, *ChemSystemsChem.* 4 (4) (2022) e202200004.
- [7] T. Ura, S. Tomita, K. Shiraki, Dynamic behavior of liquid droplets with enzyme compartmentalization triggered by sequential glycolytic enzyme reactions, *Chem. Commun.* 57 (93) (2021) 12544–12547.
- [8] R. Chollakup, W. Smitthipong, C.D. Eisenbach, M. Tirrell, Phase behavior and coacervation of aqueous poly (acrylic acid)– poly (allylamine) solutions, *Macromolecules* 43 (5) (2010) 2518–2528.
- [9] R. Chollakup, J.B. Beck, K. Dirnberger, M. Tirrell, C.D. Eisenbach, Polyelectrolyte molecular weight and salt effects on the phase behavior and coacervation of aqueous solutions of poly (acrylic acid) sodium salt and poly (allylamine) hydrochloride, *Macromolecules* 46 (6) (2013) 2376–2390.
- [10] E. Spruijt, A.H. Westphal, J.W. Borst, M.A. Cohen Stuart, J van der Gucht, Binodal compositions of polyelectrolyte complexes, *Macromolecules* 43 (15) (2010) 6476–6484.
- [11] J. van der Gucht, E. Spruijt, M. Lemmers, M.A.C. Stuart, Polyelectrolyte complexes: bulk phases and colloidal systems, *J. Colloid. Interface. Sci.* 361 (2) (2011) 407–422.
- [12] H. Bohidar, P.L. Dubin, P.R. Majhi, C. Tribet, W. Jaeger, Effects of protein– polyelectrolyte affinity and polyelectrolyte molecular weight on dynamic properties of bovine serum albumin– poly (diallyldimethylammonium chloride) coacervates, *Biomacromolecules* 6 (3) (2005) 1573–1585.
- [13] F. Mathieu, S. Ugazio, G. Carnelle, Y. Ducini, J. Legrand, Complex coacervation of the gelatin–poly (acrylic acid) system, *J. Appl. Polym. Sci.* 101 (1) (2006) 708–714.
- [14] C.E. Sing, J. Qin, Bridging field theory and ion pairing in the modeling of polyelectrolytes and complex coacervation, *Macromolecules* 56 (15) (2023) 5941–5963.
- [15] C.P. Brangwynne, T.J. Mitchison, A.A. Hyman, Active liquid-like behavior of nucleoli determines their size and shape in *Xenopus laevis* oocytes, *Proceed. Natl. Acad. Sci.* 108 (11) (2011) 4334–4339.
- [16] C.P. Brangwynne, C.R. Eckmann, D.S. Courson, A. Rybarska, C. Hoegel, J. Gharakhani, et al., Germline P granules are liquid droplets that localize by controlled dissolution/condensation, *Science* 324 (5935) (2009) 1729–1732.
- [17] F. Wippich, B. Bodenmiller, M.G. Trajkovska, S. Wanka, R. Aebersold, L. Pelkmans, Dual specificity kinase DYRK3 couples stress granule condensation/dissolution to mTORC1 signaling, *Cell* 152 (4) (2013) 791–805.
- [18] S.F. Banani, Lee HO, A.A. Hyman, M.K. Rosen, Biomolecular condensates: organizers of cellular biochemistry, *Nat. Rev. Molecul. Cell Biol.* 18 (5) (2017) 285–298.
- [19] C.J. Decker, R. Parker, P-bodies and stress granules: possible roles in the control of translation and mRNA degradation, *Cold. Spring. Harb. Perspect. Biol.* 4 (9) (2012) a012286.
- [20] Oparin A.I. The origin of life 1953.
- [21] S. Lindhoud, M.M. Claessens, Accumulation of small protein molecules in a macroscopic complex coacervate, *Soft. Matter.* 12 (2) (2016) 408–413.
- [22] F.P. Cakmak, S. Choi, M.O. Meyer, P.C. Bevilacqua, C.D. Keating, Prebiotically-relevant low polyion multivalency can improve functionality of membraneless compartments, *Nat. Commun.* 11 (1) (2020) 5949.
- [23] A.B. Cook, S. Novosedlik, J.C.M. van Hest, Complex coacervate materials as artificial cells, *Account. Mater. Res.* (2023).
- [24] J. van Lente, M.P. Urrea, T. Brouwer, B. Schuur, S. Lindhoud, Complex coacervates as extraction media, *Green Chem.* 23 (16) (2021) 5812–5824.
- [25] P.L. Dubin, J. Gao, K. Mattison, Protein purification by selective phase separation with polyelectrolytes, *Separat. Purific. Method.* 23 (1) (1994) 1–16.
- [26] Y. Wang, J.Y. Gao, P.L. Dubin, Protein separation via polyelectrolyte coacervation: selectivity and efficiency, *Biotechnol. Prog.* 12 (3) (1996) 356–362.
- [27] D.S. Kohane, Microparticles and nanoparticles for drug delivery, *Biotechnol. Bioeng.* 96 (2) (2007) 203–209.
- [28] D.J. Burgess, J.E. Carless, Microelectrophoretic studies of gelatin and acacia for the prediction of complex coacervation, *J. Colloid. Interface. Sci.* 98 (1) (1984) 1–8.
- [29] D.J. Burgess, O.N. Singh, Spontaneous formation of small sized albumin/acacia coacervate particles, *J. Pharm. Pharmacol.* 45 (7) (1993) 586–591.
- [30] F. Xing, G. Cheng, B. Yang, L. Ma, Microencapsulation of capsaicin by the complex coacervation of gelatin, acacia and tannins, *J. Appl. Polym. Sci.* 91 (4) (2004) 2669–2675.
- [31] E. Dickinson, Interfacial structure and stability of food emulsions as affected by protein–polysaccharide interactions, *Soft. Matter.* 4 (5) (2008) 932–942.
- [32] C. Schmitt, S.L. Turgeon, Protein/polysaccharide complexes and coacervates in food systems, *Adv. Colloid. Interface. Sci.* 167 (1–2) (2011) 63–70.
- [33] A. Matalanis, O.G. Jones, D.J. McClements, Structured biopolymer-based delivery systems for encapsulation, protection, and release of lipophilic compounds, *Food. Hydrocoll.* 25 (8) (2011) 1865–1880.
- [34] H.G. Bungenberg de Jong, H.R. Kruyt. Coacervation (partial miscibility in colloid systems) 1929.
- [35] Jong HB de, Die Koazervation und ihre Bedeutung für die Biologie, *Protoplasma* 15 (1) (1932) 110–173.
- [36] Bungenberg de Jong HG. Wissenschaftliche und technische Sammelreferate: Koazervation, *I. Kolloid-Zeitschrift* 1937;79(3):334–44.
- [37] L. Li, S. Srivastava, M. Andreev, A.B. Marciel, Pablo JJ de, Tirrell MV, Phase behavior and salt partitioning in polyelectrolyte complex coacervates, *Macromolecules* 51 (8) (2018) 2988–2995.
- [38] A.E. Neitzel, Y.N. Fang, B. Yu, A.M. Rumyantsev, Pablo JJ de, M.V. Tirrell, Polyelectrolyte complex coacervation across a broad range of charge densities, *Macromolecules* 54 (14) (2021) 6878–6890.
- [39] J. Wang, M.A. Cohen Stuart, J van der Gucht, Phase diagram of coacervate complexes containing reversible coordination structures, *Macromolecules* 45 (21) (2012) 8903–8909.
- [40] S. Koga, D.S. Williams, A.W. Perriman, S. Mann, Peptide–nucleotide microdroplets as a step towards a membrane-free protocell model, *Nat. Chem.* 3 (9) (2011) 720–724.
- [41] Q. Wang, J.B. Schlenoff, The polyelectrolyte complex/coacervate continuum, *Macromolecules* 47 (9) (2014) 3108–3116.
- [42] A.C. Gucinski, M.T. Boyne, D.A. Keire, Modern analytics for naturally derived complex drug substances: NMR and MS tests for protamine sulfate from chum salmon, *Anal. Bioanal. Chem.* 407 (2015) 749–759.
- [43] F. Malz, H. Jancke, Validation of quantitative NMR, *J. Pharm. Biomed. Anal.* 38 (5) (2005) 813–823.
- [44] R.W. Zwanzig, High-temperature equation of state by a perturbation method. I. Nonpolar gases, *J. Chem. Phys.* 22 (8) (1954) 1420–1426.
- [45] C. Held, T. Reschke, S. Mohammad, A. Luza, G. Sadowski, ePC-SAFT revised, *Chem. Eng. Res. Des.* 92 (12) (2014) 2884–2897.
- [46] T. Greinert, K. Vogel, J.-K. Mühlentweg, G. Sadowski, T. Maskow, C. Held, Standard Gibbs energy of metabolic reactions: VI. Glyceraldehyde 3-phosphate dehydrogenase reaction, *Fluid. Phase. Equilib.* 517 (2020) 112597.
- [47] A. Tihic, G.M. Kontogeorgis, Solms N von, M.L. Michelsen, L. Constantinou, A predictive group-contribution simplified PC-SAFT equation of state: application to polymer systems, *Ind. Eng. Chem. Res.* 47 (15) (2008) 5092–5101.
- [48] C. Held, L.F. Cameretti, G. Sadowski, Measuring and modeling activity coefficients in aqueous amino-acid solutions, *Ind. Eng. Chem. Res.* 50 (1) (2011) 131–141.
- [49] J. Vondrášek, P.E. Mason, J. Heyda, K.D. Collins, P. Jungwirth, The molecular origin of like-charge arginine– arginine pairing in water, *J. Phys. Chem. B* 113 (27) (2009) 9041–9045.

- [50] M. Vazdar, J. Heyda, P.E. Mason, G. Tesi, C. Allolio, M. Lund, et al., Arginine “magic”: guanidinium like-charge ion pairing from aqueous salts to cell penetrating peptides, *Acc. Chem. Res.* 51 (6) (2018) 1455–1464.
- [51] L.J. Prather, G.M. Weerasekare, M. Sima, C. Quinn, R.J. Stewart, Aqueous liquid-liquid phase separation of natural and synthetic polyguanidiniums, *Polym. (Basel)* 11 (4) (2019) 649.
- [52] C. Held, L.F. Cameretti, G. Sadowski, Modeling aqueous electrolyte solutions: part 1. Fully dissociated electrolytes, *Fluid. Phase. Equilib.* 270 (1–2) (2008) 87–96.
- [53] A. Wangler, R. Loll, T. Greinert, G. Sadowski, C. Held, Predicting the high concentration co-solvent influence on the reaction equilibria of the ADH-catalyzed reduction of acetophenone, *J. Chem. Thermodyn.* 128 (2019) 275–282.